Magnetic resonance imaging biomarkers of chronic obstructive pulmonary disease prior to radiation therapy for non-small cell lung cancer

Khadija Sheikh [a,b,1], Dante P.I. Capaldi [a,b,1], Douglas A. Hoover [c], David A. Palma [c], Brian P. Yaremko [c], Grace Parraga [a,b,c,*]

[a] *Imaging Research Laboratories, Robarts Research Institute, London, Canada*
[b] *Department of Medical Biophysics, The University of Western Ontario, London, Canada*
[c] *Department of Oncology, The University of Western Ontario, London, Canada*

Abstract

Objective: In this prospectively planned interim-analysis, the prevalence of chronic obstructive lung disease (COPD) phenotypes was determined using magnetic resonance imaging (MRI) and X-ray computed tomography (CT) in non-small-cell-lung-cancer (NSCLC) patients.

Materials and methods: Stage-III-NSCLC patients provided written informed consent for pulmonary function tests, imaging and the 6-min-walk-test. Ventilation defect percent (VDP) and CT lung density (relative-of-CT-density-histogram <-950, RA_{950}) were measured. Patients were classified into three subgroups based on qualitative and quantitative COPD and tumour-specific imaging phenotypes: (1) tumour-specific ventilation defects (TSD), (2) tumour-specific and other ventilation defects without emphysema (TSD_V), and, (3) tumour-specific and other ventilation defects with emphysema (TSD_{VE}).

Results: Seventeen stage-III NSCLC patients were evaluated (68 ± 7 years, 7 M/10 F, mean $FEV_1 = 77\%_{pred}$) including seven current and 10 ex-smokers and eight patients with a prior lung disease diagnosis. There was a significant difference for smoking history ($p = .02$) and FEV_1/FVC ($p = .04$) for subgroups classified using quantitative imaging. Patient subgroups classified using qualitative imaging findings were significantly different for emphysema (RA_{950}, $p < .001$). There were significant relationships for whole-lung VDP ($p < .05$), but not RECIST or tumour-lobe VDP measurements with pulmonary function and exercise measurements. Preliminary analysis for non-tumour burden ventilation abnormalities using Reader-operator-characteristic (ROC) curves reflected a 94% classification rate for smoking pack-years, 93% for FEV_1/FVC and 82% for RA_{950}. ROC sensitivity/specificity/positive/negative likelihood ratios were also generated for pack-years, (0.92/0.80/4.6/0.3), FEV_1/FVC (0.92/0.80/4.6/0.3), RA_{950} (0.92/0.80/4.6/0.3) and RECIST (0.58/0.80/2.9/1.1).

Conclusions: In this prospectively planned interim-analysis of a larger clinical trial, NSCLC patients were classified based on COPD imaging phenotypes. A proof-of-concept evaluation showed that FEV_1/FVC and smoking history identified NSCLC patients with ventilation abnormalities appropriate for functional lung avoidance radiotherapy.

© 2015 The Authors. Published by Elsevier Ltd. This is an open access article under the CC BY-NC-ND license (http://creativecommons.org/licenses/by-nc-nd/4.0/).

Keywords: Lung; Cancer; COPD; Phenotype; Radiotherapy; Functional magnetic resonance imaging

1. Introduction

The current standard of care for patients with non-small cell lung cancer (NSCLC) relies on radiation therapy that focuses the radiation dose to the tumour, sparing healthy lung tissue. However, the current standard approach for radiation therapy planning uses four-dimensional computed tomography (4DCT) to delineate the target volume and this does not take into account lung function heterogeneity. This is an important consideration, especially in ex-smokers with chronic obstructive pulmonary disease (COPD) or other underlying lung disease. In these patients, pulmonary functional imaging has been used to characterize large functional deficits of poorly and unventilated lung [1,2] which is typically very spatially heterogeneous. Moreover,

such functional defects cannot be easily predicted by smoking history or other pulmonary function measurements, including the forced expiratory volume in 1 second (FEV$_1$) [1,3,4]. Ideally, radiation treatment planning should derive improvements from pulmonary imaging measurements that differentiate the functioning from non-functioning lung, with attention focused on the non-functioning part of the lung, independent of tumour burden.

Pulmonary functional imaging methods such as single photon emission computed tomography (SPECT) [5,6], 4DCT [7,8] and inhaled gas magnetic resonance imaging (MRI) [9,10], have been previously incorporated in functional imaging lung avoidance schemes, but this approach is not currently the standard clinical practice. The feasibility of function-based intensity modulated radiation therapy (IMRT) treatment planning [5,6,9], has been demonstrated, in addition to measurements of lung function before and after radiation treatment [7,11]. Importantly, when functional imaging was used to guide therapy in radiation planning studies, dose reductions to functioning lung were achievable [6,10]. Previous work also identified that functional lung avoidance plans can be optimized in patients with bullous lung disease and large perfusion defects [12,13].

While these thoracic imaging techniques provide a way to differentiate between functioning and non-functioning lung, there are a number of inherent limitations that have restricted the use of functional imaging for radiation therapy planning. For example, with SPECT imaging, artefacts stemming from radiolabelled tracers are typically observed in the major airways [14]. For 4DCT [15], lung function is indirectly measured over a time series of breaths and the resultant lung function maps require extensive image processing that is highly dependent on deformable image registration [16,17]. Fourier-decomposition 4D MRI is an alternative imaging method that indirectly measures lung ventilation and perfusion and correlates well with other pulmonary functional MR methods [18]. On the other hand, hyperpolarized noble gas MRI, although very sensitive to functional ventilation abnormalities, is limited because of its reliance on specialized MRI and polarization equipment. While the global quantities of ^{3}He are very limited and expensive, impeding its clinical uptake and translation, the sensitivity of this method may guide the use of other MR methods (e.g. Fourier decomposition, ^{129}Xe MRI, etc.). In addition, although MRI methods are well-tolerated, making them ideal for serial studies [19], until now, these methods have been limited to research applications only.

Therefore, in an interim analysis of a larger clinical trial [20], the objective of this proof-of-concept evaluation was to quantify imaging phenotypes of COPD in patients with NSCLC prior to concurrent chemo- and radiation therapy. We aimed to determine the utility of conventional and clinically available COPD measurements in stratifying patients for functional lung avoidance radiotherapy. We hypothesized that COPD phenotypes could be used to stratify NSCLC patients prior to radiotherapy planning as a first step towards personalizing treatment plans based on lung structural and functional measurements.

2. Materials and methods

2.1. Study participants

Study participants were evaluated in a prospectively planned interim analysis of a clinical trial in over 60 patients [20]. The logistical details of this clinical trial (NCT02002052) were previously published [20]; here we provide an interim analysis of the feasibility of acquiring and quantifying MRI phenotypes prior to randomization to standard or individualized functional lung avoidance radiation treatment. Volunteers with histologically confirmed non-resectable Stage IIIA or IIIB NSCLC and a smoking history of >10 pack-years provided written informed consent to this randomized controlled clinical trial which complied with the Health Insurance Portability and Accountability Act (HIPAA) and Personal Information Protection and Electronic Documents Act (PIPEDA), and approved by our local research ethics board and by Health Canada. Briefly, all subjects were required to be over 18 years of age, with an Eastern Cooperative Oncology Group (ECOG) performance score between 0 and 2, FEV$_1$ > 30%$_{pred}$, and able to undergo platinum-based chemotherapy as determined by his/her treating physicians. Those subjects with contradictions to the MRI (i.e. metal/electronic/magnetic implants, claustrophobia, etc.), serious co-morbidities, prior thoracic radiation, metastatic disease, or conflicts with routine radiotherapy were not considered suitable for the study. In addition to routine clinical care, in a two and a half hour visit, all study volunteers underwent additional pulmonary function tests, MRI, one additional low dose inspiratory CT, and the 6 min walk test (6MWT) [20].

2.2. Pulmonary function tests

Spirometry was used to acquire the forced expiratory volume in one second (FEV$_1$), forced vital capacity (FVC), and FEV$_1$/FVC according to American Thoracic Society (ATS) guidelines (Medgraphics Elite Series Plethysmograph, MedGraphics Corporation, St. Paul, MN, USA) [21]. Body plethysmography was also performed to measure lung volumes and the diffusing capacity of carbon monoxide (DL$_{CO}$) was also measured using the attached gas analyser (Medgraphics Elite Series Plethysmograph).

2.3. Image acquisition

MRI was acquired in the coronal plane using a whole body 3.0 Tesla Discovery MR750 (General Electric Health Care, Milwaukee, WI) system with broadband imaging capability. Polarization of the ^{3}He/^{129}Xe gas was performed using a polarizer system (HeliSpin/XeniSpin; Polarean, Durham, NC, USA) and achieved polarization levels of approximately 40%/8%. Hyperpolarized ^{3}He was diluted with medical-grade N$_2$ gas (Spectra Gases, NJ, USA) and ^{129}Xe was diluted with ^{4}He/N$_2$ and administered in 1.0-L Tedlar$^®$ bags (Jensen Inert Products, FL, USA). Subjects were instructed to inhale a gas mixture from the bag from functional residual capacity (FRC) and image acquisition was performed under

breath-hold conditions [22]. [1]H MRI was acquired with subjects in breath-hold using a whole-body radiofrequency coil and a ^{1}H fast spoiled gradient-recalled echo (FGRE) sequence with a partial echo (16 s total data acquisition, repetition time [TR]/echo time [TE]/flip angle = 4.7 ms/1.2 ms/30°, field-of-view [FOV] = 40 cm × 40 cm, bandwidth [BW] = 24.4 kHz, matrix = 128 × 80, 15–17 slices, 15 mm slice thickness, 0 gap), as previously described [22]. Hyperpolarized [3]He MRI static ventilation imaging was performed using a 2D multi-slice fast gradient-recalled echo sequence with a partial echo (total data acquisition time = 10 s; TR/TE/flip-angle = 3.8 ms/1.0 ms/7°; FOV = 40 cm × 40 cm; matrix = 128 × 80; BW = 62.50 kHz; number of excitations [NEX] = 1; number of slices = 16; slice thickness = 15 mm) during breath hold [22]. Hyperpolarized [129]Xe MRI static ventilation imaging was performed to determine whether it provided similar or additional information to [3]He MRI. [129]Xe MRI was performed using a 3D FGRE sequence (total data acquisition time = 16 s; TR/TE/flip-angle = 7.0 ms/1.8 ms/variable; FOV = 40 cm × 40 cm; matrix = 128 × 128; BW = 9 kHz; NEX = 1; number of slices = 16; slice thickness = 15 mm) during a breath-hold. The time duration between [3]He and [129]Xe was 10–15 min. The subject was removed from the bore of the MRI to allow for the coils to be switched. The subject was re-localized, ^{1}H MRI was performed followed by [129]Xe MRI.

Thoracic CT images were acquired at FRC + 1 L using a multi-detector, 64-slice Lightspeed VCT scanner (General Electric Health Care, Milwaukee, WI) (64 mm × 0.625 mm collimation, 120 kVp, 100 effective mA, tube rotation time = 500 ms, pitch = 1.0) [23]. A spiral acquisition was used and images reconstructed using a standard convolution kernel to 1.25 mm [23].

2.4. Image analysis

Noble gas static ventilation images were segmented and registered to the ^{1}H MRI thoracic cavity using custom software we previously generated using MATLAB R2014a (Mathworks, Natrick, MA, USA), as previously described [24]. Ventilation abnormalities were quantified using the ventilation defect percent (VDP) which represents the volume of ventilation defects (VDV) normalized to the thoracic cavity volume (TCV). Briefly, [3]He static ventilation images were segmented by a single observer (K.S. with three years of experience performing semi-automated segmentation and a coefficient of variation of 4%) using a k-means approach that classified voxel intensity values into five clusters ranging from signal void (cluster 1[C1] or VDV) and hypo-intense (cluster 2 [C2]) to hyper-intense signal (cluster 5 [C5]), therefore, generating a gas distribution cluster-map. For delineation of the ventilation defect boundaries, a seeded region-growing algorithm was used to segment the ^{1}H MRI thoracic cavity for registration to the cluster-map, as previously described [24].

Pulmonary Workstation 2.0 (VIDA Diagnostics Inc., Coralville, IA, USA) was used to quantify the relative area of the CT density histogram with attenuation values < −950 HU

(RA_{950}) as well as segmenting the lungs and lobes. Using the pulmonary lobe masks produced by VIDA, the VDP for each pulmonary lobe was determined by applying these masks to the static ventilation images. Ventilation defect percent was calculated for the tumour lobe(s) (VDP_{TL}) and the lobes with no tumour (VDP_{NTL}). VDP_{TL} was generated by normalizing the ventilation defect volume for a specific lobe to the corresponding lobe volume. Similarly, the VDP_{NTL} was generating by normalizing the ventilation abnormalities of the non-tumour lobe(s) to the corresponding lobar volume(s). Finally, the Response Evaluation Criteria in Solid Tumours (RECIST) was evaluated [25].

Subjects were classified into three sub-groups based on qualitative and quantitative imaging evidence of ventilation defects and emphysema: (1) subjects with tumour-specific ventilation defects (TSD), (2) subjects with tumour-specific and other ventilation defects with no emphysema (TSD_V), and, (3) subjects with tumour-specific and other ventilation defects with emphysema (TSD_{VE}). Three observers ((a) G.P. with 10 years of experience, (b) K.S. with three years of experience, and (c) D.P.I.C. with two years of experience analyzing noble gas MRI and CT) in a consensus decision, qualitatively evaluated and classified all subjects based on the visible evidence of tumour and non-tumour lobe ventilation defects and on the presence of emphysema. For qualitative analyses, all image slices were evaluated using 3D Slicer 4.2 open-source platform (http://www.slicer.org, Boston, MA) as the visualization environment and with flexible windows and levels for ventilation and emphysema extent. For quantitative classification of subjects, the upper limit of the 95% confidence interval of VDP measurements from a previously published [26] study in healthy volunteers was used as the threshold (>3%) for ventilation defects. Subjects with ventilation defects in the tumour lobe only (non-tumour lobes: VDP < 3%) were classified in the TSD subgroup. Subjects with ventilation defects in non-tumour lobes (VDP > 3%) were classified in the TSD_V subgroup. For those subjects with non-tumour lobe ventilation defects, the value of $RA_{950} \geq 5\%$ was used to further stratify these subjects into the TSD_{VE} subgroup [27].

2.5. Statistical analysis

A one-way analysis of variance (ANOVA) with post hoc Tukey HSD (Honest Significant Differences) and Pearson correlation coefficients (r) were used to determine the relationships between measurements using SPSS Statistics V22.0 (SPSS Inc., IBM Corporation, Armonk, NY, USA). Results were considered significant when the probability of two-tailed type I error (α) was less than 5% ($p < .05$). Receiver-operating characteristic (ROC) curves were used to characterize the performance of pulmonary function test and other clinical measures as predictors of the presence of ventilation defects not associated with tumour burden (control group: TSD sub-group; patient group: TSD_V and TSD_{VE} sub-groups). The maximum Youden's J index value (J = sensitivity + specificity-1) was used to determine the optimum cut-off point and the corresponding sensitivity, specificity, positive and negative likelihood ratios
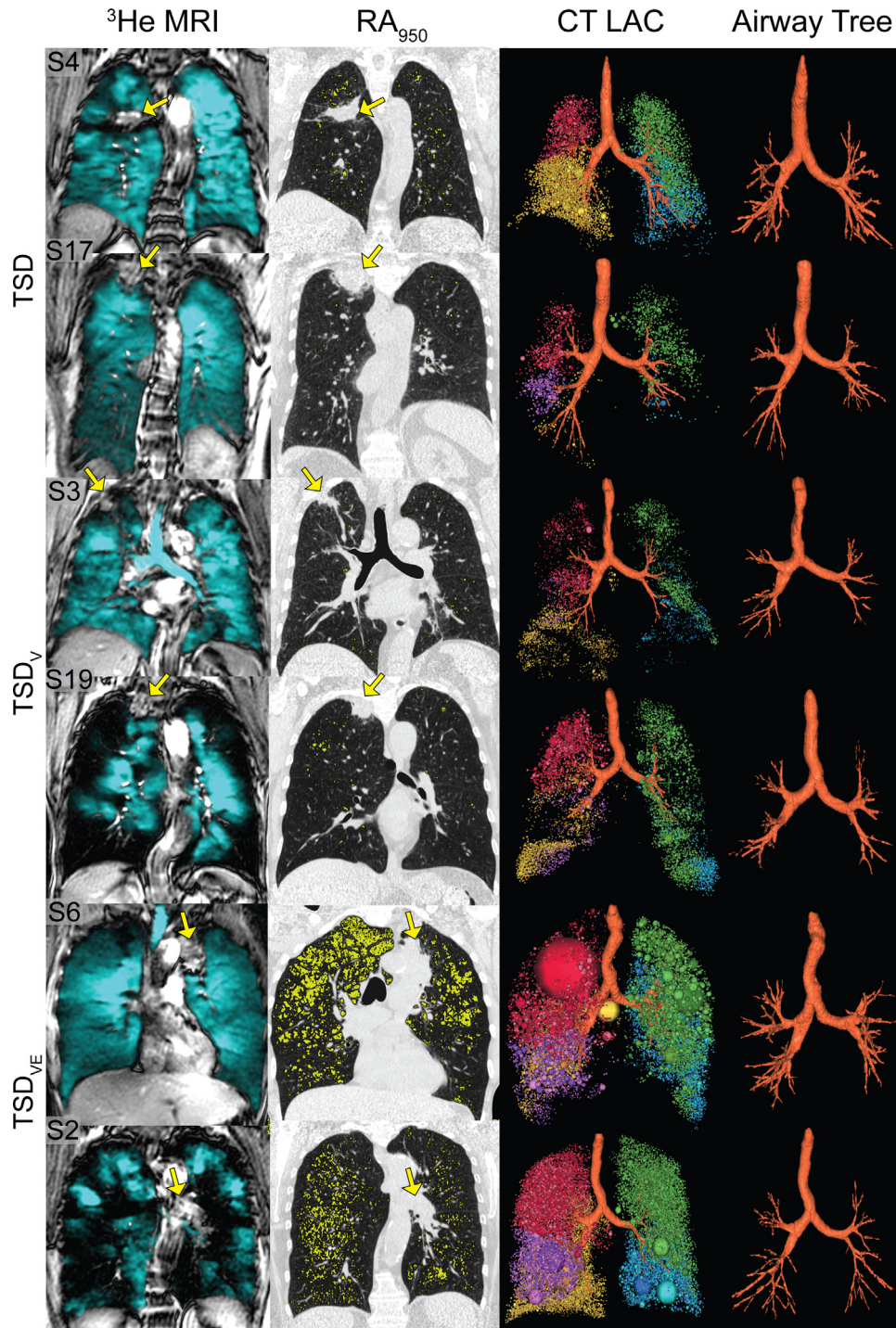
Fig. 1. ^{3}He MRI and CT for representative subjects with tumour-specific ventilation defects (TSD), tumour-specific and other ventilation defects (TSD$_V$), without emphysema, and tumour-specific and other ventilation defects with emphysema (TSD$_{VE}$) based on quantitative analysis. Left: ^{3}He MRI coronal static ventilation in blue co-registered to ^{1}H MRI. Middle: CT density masks where *yellow* = attenuation < −950 Hounsfield units (RA$_{950}$). Right: CT three-dimensional low-attenuation clusters (LAC), represented as spheres with CT densitometry values < −950 HU and CT three-dimensional reconstruction airway tree. Yellow arrows indicate tumour location. (For interpretation of the references to colour in this figure legend, the reader is referred to the web version of this article.)

were calculated. It should be noted that to demonstrate a significant Reader Operator curve result with the same number of positive and negative cases, the required sample size is 26 [28]. The ROC analysis statistics were performed using GraphPad Prism version 6.02 (GraphPad, Inc., San Diego, CA, USA).

3. Results

3.1. Participants

Twenty-three subjects consented to the study, but only 17 completed MRI and pulmonary function tests (PFTs) and were

Table 1
Subject listing and classification.

	Sex	Age (y)	Pack-years	Current smoker	Tumour location	Previously diagnosed lung disease	Quantitative classification	Qualitative classification
001	F	62	50	N	RLL	COPD	TSD_{VE}	TSD_{VE}
002	F	69	50	N	LLL	COPD	TSD_{VE}	TSD_{VE}
003	M	67	50	N	RUL	None	TSD_V	TSD_V
004	F	68	35	N	RUL	COPD	TSD	TSD_V
006	M	71	50	Y	LUL	COPD	TSD_{VE}	TSD_{VE}
007	F	63	50	Y	RUL	None	TSD_V	TSD_V
008	F	70	45	Y	RUL	None	TSD	TSD
010	F	65	35	N	RML	None	TSD_V	TSD_V
011	F	56	42	Y	LLL	COPD	TSD_V	TSD_V
012	M	72	50	N	LLL	COPD	TSD_{VE}	TSD_{VE}
013	F	62	10	N	RUL	None	TSD	TSD_V
015	F	79	30	Y	LLL	None	TSD	TSD_V
017	F	67	30	N	RUL	Asthma	TSD	TSD_V
019	M	68	53	Y	RUL	None	TSD_V	TSD_V
020	M	59	40	N	RML	None	TSD_{VE}	TSD_{VE}
021	M	81	70	N	LUL	None	TSD_V	TSD_V
023	M	74	90	Y	LUL	COPD	TSD_V	TSD_V
Mean	7 M/10 F	68	46	7 Y/10 N		7 COPD/ 1 Asthma/ 9 none	5 TSD/ 7 TSD_V/ 5 TSD_{VE}	1 TSD/11 TSD_V/5 TSD_{VE}

RLL = right lower lobe; RUL = right upper lobe; RML = right middle lobe; LLL = left lower lobe; LUL = left upper lobe; TSD = tumour-specific ventilation defects only; TSD_V = tumour-specific and other ventilation defects with no emphysema; TSD_{VE} = tumour-specific and other ventilation defects with emphysema.

included in this analysis. The six subjects who consented but did not complete evaluations were unable to participate because of difficulties in travel conditions to the site (snowstorm). Table 1 shows a subject listing for the 17 subjects (68 ± 7 years, 7 M/10 F) who completed baseline imaging and pulmonary function measurements and participant classification according to both qualitative and quantitative imaging phenotypes. All subjects were diagnosed with locally advanced Stage IIIA or IIIB NSCLC according to the American Joint Committee on Cancer (7th edition) [29] with a smoking history of >10 pack-years (46 ± 17 pack-years). Of the 17 subjects who completed baseline measurements, seven were current smokers and ten were ex-smokers with a mean years-quit of 16 ± 13 years. Eight subjects had a prior diagnosis of lung disease. Nine patients reported $FEV_1/FVC < 70\%$ and four patients reported $FEV_1 < 50\%_{pred}$.

3.2. Imaging and other measurements by subgroup

Fig. 1 shows the coronal ^{3}He static ventilation image with the corresponding RA_{950} map, CT low attenuation cluster (LAC) map and the airway tree for six representative subjects, including: (1) S4 and S17 with quantitative tumour-specific ventilation defects only, (2) S3 and S19 with quantitative tumour-specific and other ventilation defects, and, (3) S2 and S6 with quantitative tumour-specific and other ventilation defects with comorbid emphysema. Yellow arrows show the location of tumour masses. Specifically, subjects S4 and S17 in the TSD subgroup showed homogeneous regions of ventilation, except for the regions near the tumour, where obvious ventilation abnormalities were clearly visible. Qualitatively, these two subjects also showed more complete airway trees than those subjects in the TSD_V and TSD_{VE} subgroup. Subjects in the TSD_V and TSD_{VE} subgroups

had numerous and large ventilation defects related to the tumour and also in non-tumour regions of interest. For the two representative participants (S2 and S6) in the TSD_{VE} subgroup there was visible evidence of significant centrilobular emphysema as reflected in the RA_{950} and low attenuating cluster maps.

Table 2 shows subject demographics, pulmonary function and 6MWT measurements for all participants and the three qualitative and quantitative comparator subgroups. There were no significant differences among the qualitatively determined subgroups, except for RA_{950} ($p < .001$). In the quantitatively determined subgroups, there were significant differences for FEV_1/FVC ($p = .04$) and smoking history ($p = .02$). Post hoc analysis showed that the TSD_V subgroup had significantly different FEV_1/FVC ($p = .04$), and smoking history ($p = .02$) than the TSD subgroup.

3.3. Univariate relationships

As shown in Table 3 for all measurements and in detail in Fig. 2, there were significant relationships for whole lung VDP with pulmonary function (FEV_1, FEV_1/FVC, IC, and FRC), DL_{CO}, 6MWD, and pre-6MWT oxygen saturation measurements but not RECIST or RA_{950} measurements. For tumour-lobe VDP, there was a significant relationship with pre-6MWT SpO_2 while for non-tumour-lobe VDP there was a significant relationship with pulmonary function measurements (FEV_1/FVC and FRC). Finally, RA_{950} was significantly related to FRC and the longest tumour diameter RECIST measurement was significantly related to VDP_{TL}. Fig. 2 shows the significant relationships for VDP with SpO_2, VDP_{NTL} with FRC and FEV_1/FVC and finally RA_{950} with FRC.

Table 2
Subject demographics, pulmonary function test, and imaging measurements.

Mean (±SD)	All	Quantitative classification				Qualitative classification			
	($n = 17$)	TSD ($n = 5$)	TSD$_V$ ($n = 7$)	TSD$_{VE}$ ($n = 5$)	p-value	TSD ($n = 1$)	TSD$_V$ ($n = 11$)	TSD$_{VE}$ ($n = 5$)	p-value
Age yrs	68 (7)	69 (6)	68 (8)	67 (6)	.9	70	68 (7)	67 (6)	.9
Male n	7	0	4	3	–	0	4	3	–
BMI kg/m^2	28 (4)	27 (4)	29 (4)	28 (6)	.8	25	28 (4)	28 (6)	.8
Pack years	46 (17)	**30 (13)**	**56 (19)**	**48 (4)**	**.02**	45	45 (22)	48 (4)	~1
Lung disease n	8	2	2	4	–	0	4	4	–
RECIST mm	49 (22)	54 (21)	40 (25)	57 (18)	.4	90	42 (20)	57 (18)	.07
FEV$_1$%$_{pred}$	77 (28)	94 (14)	68 (27)	72 (36)	.3	77	79 (26)	72 (36)	.9
FEV$_1$/FVC %	65 (10)	**75 (3)**	**61 (8)**	**62 (13)**	**.04**	71	66 (10)	62 (13)	.7
IC %$_{pred}$	86 (22)	100 (20)	83 (21)	76 (22)	.2	113	88 (21)	76 (22)	.3
FRC %$_{pred}$	116 (27)	97 (10)	117 (27)	134 (30)	.08	105	109 (24)	134 (30)	.2
DL$_{CO}$ %$_{pred}$	55 (18)	57 (20)	60 (13)	45 (22)	.4	46	60 (16)	45 (22)	.3
SpO$_2$%	95 (5)	98 (2)	95 (5)	91 (8)	.2	98	96 (4)	91 (8)	.2
6MWD m	355 (77)	372 (78)	360 (47)	331 (115)	.7	313	370 (59)	331 (115)	.6
VDP %	13 (10)	7 (4)	13 (11)	20 (9)	–	13	10 (10)	19 (9)	.3
VDP$_{TL}$ %	26 (24)	23 (25)	17 (13)	41 (32)	–	60	16 (14)	41 (32)	.05
VDP$_{NTL}$ %	8 (9)	1 (1)	10 (12)	12 (8)	–	1	7 (10)	12 (8)	.5
RA$_{950}$%	4 (4)	1 (1)	1 (1)	9 (3)	–	**1**	**1 (1)**	**9 (3)**	**<.001**

Bold values represent significant differences.
TSD = tumour-specific ventilation defects only; TSD$_V$ = tumour-specific and other ventilation defects with no emphysema; TSD$_{VE}$ = tumour-specific and other ventilation defects with emphysema; Sig Dif = Significant difference between subgroups ($p < .05$) determined by ANOVA; SD = standard deviation; %$_{pred}$ = percent predicted; BMI = body mass index; Lung disease = previously diagnosed lung disease; RECIST = Response Evaluation Criteria in Solid Tumours baseline longest diameter; FEV$_1$ = forced expiratory in 1 s; FVC = forced vital capacity; IC = inspiratory capacity; FRC = functional residual capacity; DL$_{CO}$ = diffusing capacity of carbon monoxide; SpO$_2$ = pre-6MWT digital oxygen saturation value 6MWT = 6 min walk test; 6MWD = distance travelled in 6 min; VDP = ventilation defect percent; TL = tumour lobe; NTL = non-tumour lobes; RA$_{950}$ = relative area of the lung with attenuation values < −950 HU.

Table 3
Univariate relationships between imaging measurements and pulmonary function, smoking history, and 6MWT measurements.

	VDPr (p-value)	VDP$_{NTL}r$ (p-value)	VDP$_{TL}r$ (p-value)	RA$_{950}r$ (p-value)	RECISTr (p-value)
FEV$_1$%$_{pred}$	**−0.58 (.02)**	−0.47 (.06)	−0.25 (.3)	−0.06 (.8)	−0.10 (.7)
FEV$_1$/FVC %	**−0.51 (.04)**	**−0.73 (.001)**	−0.07 (.8)	−0.33 (.2)	−0.12 (.7)
IC %$_{pred}$	**−0.64 (.01)**	−0.45 (.07)	−0.30 (.3)	−0.17 (.2)	−0.03 (.9)
FRC %$_{pred}$	**0.51 (.04)**	**0.74 (.001)**	0.19 (.5)	**0.50 (.04)**	0.003 (.9)
DL$_{CO}$ %$_{pred}$	**−0.54 (.03)**	−0.11 (.7)	−0.46 (.06)	−0.28 (.3)	−0.27 (.3)
SpO$_2$%	**−0.71 (.001)**	−0.34 (.2)	**−0.56 (.02)**	−0.30 (.3)	−0.32 (.2)
6MWD m	**−0.50 (.04)**	−0.05 (.8)	−0.48 (.05)	−0.07 (.8)	−0.18 (.5)
Pack−years yr	0.34 (.2)	0.25 (.3)	0.13 (.6)	0.16 (.5)	0.29 (.3)
VDP$_{TL}$ %	**0.59 (.01)**	0.16 (.5)	–	0.10 (.7)	**0.53 (.03)**

Bold values represent significant correlations.
VDP = ventilation defect percent; NTL = non-tumour lobes; TL = tumour lobe; RA$_{950}$ = relative area of the lung with attenuation values < −950 HU; RECIST = Response Evaluation Criteria in Solid Tumour longest diameter; SpO$_2$ = pre-6MWT digital oxygen saturation value; 6MWD = 6 min walk distance.

3.4. ROC analysis

In Fig. 3, we evaluated a number of different measurements as discriminants of patients with and without ventilation abnormalities beyond the tumour region-of-interest using ROC curves. FEV$_1$/FVC and pack-years were evaluated because these two measurements were significantly different for the quantitatively determined subgroups. RA$_{950}$ was also evaluated in order to ascertain the role of underlying emphysema in discriminating patients. Tumour RECIST measurements were also evaluated because these measurements are commonly used to reflect tumour burden. Pack-years (AUC = 0.94, 95% CI = 0.83–1.06, $p = .005$), FEV$_1$/FVC (AUC = 0.93, 95% CI = 0.82–1.05, $p = .006$) and RA$_{950}$ (AUC = 0.82, 95%

CI = 0.58–1.06, $p = .04$) significantly discriminated NSCLC patients with additional non-tumour specific ventilation defects, but RECIST measurements (AUC = 0.60, 95% CI = 0.32–0.88, $p = .5$) did not. Furthermore, for each diagnostic measurement, the established cut-off point and the corresponding performance characteristics (sensitivity, specificity, positive and negative likelihood ratios) were: pack-years: >37.5 years, 0.92, 0.80, 4.6, 0.3; FEV$_1$/FVC: <73.5%, 0.92, 0.80, 4.6, 0.3; RA$_{950}$: >1.15%, 0.92, 0.80, 4.6, 0.3; RECIST: <45.5 mm, 0.58, 0.8, 2.9, 1.1.

4. Discussion

To better understand the feasibility of pulmonary imaging structure–function phenotyping of patients prior to radiation
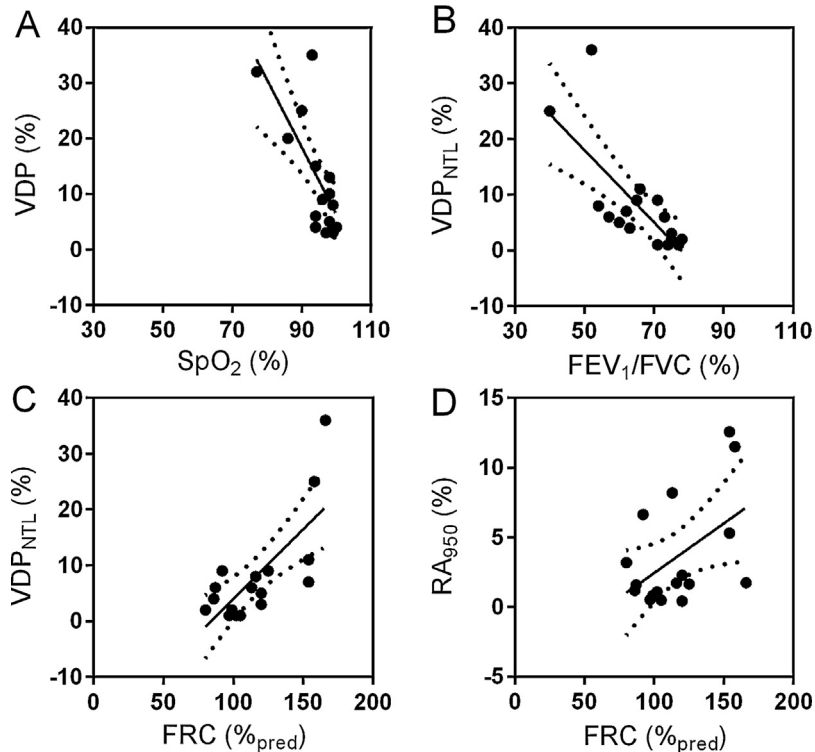
Fig. 2. Univariate relationships for imaging measurements and other measurements. (A) VDP and SpO_2 ($r = -0.71$, $p = .001$), (B) VDP_{NTL} and FEV_1/FVC ($r = -0.73$, $p = .001$), (C) VDP_{NTL} and FRC ($r = 0.74$, $p = .001$), and, (D) RA_{950} and FRC ($r = 0.50$, $p = .04$). The dotted lines represent the 95th confidence interval of the regression lines.
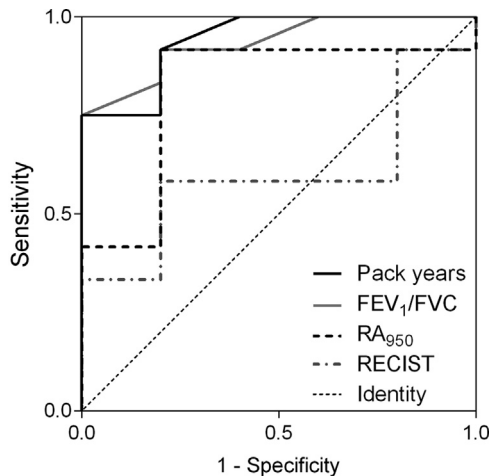

Fig. 3. Receiver-operating characteristic curves for the identification of ventilation defects not associated with the tumour using pack-years (black solid line), FEV_1/FVC, (dark grey solid line), RA_{950}, (black dashed line), and RECIST longest diameter (dark grey dashed line). The area under the curve, [95% confidence interval], (p-value) were: pack-years = 0.94, [0.83–1.06] ($p = .005$); $FEV_1/FVC = 0.93$ [0.82–1.05], ($p = .006$); $RA_{950} = 0.82$, [0.58–1.05], ($p = .04$), and; RECIST = 0.60, [0.32–0.88], ($p = .5$).

therapy planning, we evaluated 17 Stage III NSCLC subjects based on regional ventilation heterogeneity and emphysema measurements before their radiation therapy plans were formulated. We made a number of observations including: (1) three different subgroups were quantitatively and qualitatively identified based on the presence of tumour-specific ventilation

abnormalities, and COPD-biomarkers such as non-tumour ventilation abnormalities and emphysema, (2) for quantitatively identified subgroups, there were significant differences for pack-years and FEV_1/FVC, but not tumour RECIST measurements, and for qualitatively identified subgroups, there was a significant RA_{950} difference, (3) whole lung and non-tumour lobe VDP were significantly correlated with pulmonary function test measurements, but tumour lobe VDP and RECIST measurements were not, and, (4) ROC analysis identified smoking pack-years, FEV_1/FVC, and RA_{950} as diagnostics for non-tumour burden imaging findings reflective of COPD.

We used quantitative pulmonary imaging to classify patients based on the extent of underlying COPD and independent of pulmonary function tests. Three different subgroups were identified and it was somewhat unexpected that not all NSCLC patients with a previous diagnosis of asthma or COPD exhibited the ventilation heterogeneity commonly observed in COPD subjects [1,2]. The premise of functional lung avoidance radiation therapy is the specific targeting of regional non-functioning lung, so subjects with no ventilation heterogeneity would not be good candidates for this approach, as previously described using SPECT perfusion imaging [13]. This finding has had a profound effect on our original plan to randomize all NSCLC patients to either standard or individualized radiation therapy planning because only a subgroup of patients exhibited COPD phenotypes such as ventilation heterogeneity and emphysema that could be used in the radiation treatment planning process.

We also evaluated the practicality of using *qualitative* imaging phenotypes of COPD and noted that the composition of the

three subgroups was markedly different with respect to patients with tumour-specific and other defects. These results can be explained by the semi-automated segmentation tool used for quantitative analysis of noble gas MRI ventilation. As previously described [24], an expert observer can distinguish between four visually different classes of ^{3}He MRI gas signal including: signal void, hypointense regions, normal intensity, and hyperintense signal [24]. Quantitative segmentation depends on k-means clustering that identifies two distinct clusters (signal void and hypointense clusters), but visually, these regions appear as signal void. Therefore patients with visibly obvious ventilation defects may not meet the threshold for ventilation defect percent. This is evident by the fact that there were more subjects with qualitatively as compared to quantitatively identified ventilation defects. Regardless, for the two different types of subgroups, there were no significant differences observed for pulmonary function, 6 min walk test or MRI measurements, although emphysema (RA_{950}) was significantly different. These results lead us to believe that ventilation defects may be due to a combination of small airway occlusion, mucous plugs, airway wall thickening and inflammation or bullous disease, which are common in COPD [30,31]. These results also suggest that qualitative analysis may not be appropriate for phenotyping COPD patients, supporting the need for quantitative analysis or the use of novel biomarkers [32] not investigated here.

It is interesting to note that whole lung and non-tumour lobe VDP were significantly correlated with pulmonary function test measurements, but baseline RECIST measurements and VDP_{TL} did not. These results are consistent with previous findings which reported a relationship for increased hyperpolarized gas MRI ventilation heterogeneity with poor lung function and exercise capacity in COPD [1,33]. To determine if the diminished pulmonary function observed in these subjects was due to tumour burden or the underlying COPD, we determined the relationships for VDP in the tumour lobe and non-tumour lobes. The fact that VDP in the non-tumour lobes was related to pulmonary function test measurements reinforces the notion that tumour burden alone does not explain airflow and exercise limitation in NSCLC subjects.

Finally, among the three quantitatively identified subgroups, there were significant differences for smoking history (pack-years) and FEV_1/FVC, but not for exercise capacity or tumour RECIST measurements. This supports the idea that the airflow limitation observed in NSCLC patients is contributed by a combination of the tumour burden, airways disease and emphysema, similar to what was previously observed in COPD subjects [1,34]. Importantly, ROC analysis estimated a classification rate of 94% for pack-years and 93% for FEV_1/FVC when discriminating patients based on COPD imaging phenotypes. Smoking history measured in pack-years, as well as FEV_1/FVC, and RA_{950} showed 92% sensitivity (true positives) and 80% specificity (true negatives). The likelihood ratios for these diagnostic measurements also suggested that NSCLC patients with a positive test (i.e. pack-years > 37.5 years, FEV_1/FVC < 73.5%, RA_{950} > 1.15%) were approximately five times more likely to have COPD-like ventilation abnormalities as NSCLC patients with a negative test (i.e. pack-years < 37.5 years, FEV_1/FVC > 73.5%, RA_{950} < 1.15%). This strongly suggests that FEV_1/FVC, pack-years, and RA_{950} can be used as diagnostics for COPD-related ventilation abnormalities in patients with NSCLC. Although these measures had similar sensitivity and specificity, the AUC suggested different classification rates for FEV_1/FVC and pack-years (classification rates of 93% and 94%, respectively) versus RA_{950} (classification rate of 82%). We also acknowledge that the sample size for the interim ROC analysis was smaller than typically required to determine significant predictors, so caution must be used in its interpretation and the results should be considered exploratory and hypothesis generating. Certainly, once the clinical trial is completed, 64 subjects will be evaluated and the results of the interim analysis will help guide recruitment to appropriately test our hypotheses.

We recognize that because of the expense and limited quantities of ^{3}He gas, alternative pulmonary imaging methods such as ^{129}Xe MRI and Fourier decomposition MRI should be optimized and utilized to provide similar lung structure–function COPD measurements. It is also important to note that these subjects were classified based on the presence of ventilation defects and emphysema without regard to the location of the tumour with respect to the ventilation defects and emphysematous regions. Unfortunately, due to the small sample size in this study, categorizing these subjects based on tumour location was not feasible. Future work should incorporate this information when phenotyping subjects for functional lung avoidance radiation therapy.

5. Conclusions

In summary, we classified NSCLC subjects into three subgroups based on imaging measurements of ventilation heterogeneity and the presence of emphysema. In this proof-of-concept analysis, pulmonary imaging was used to phenotype NSCLC patients on the basis of underlying COPD biomarkers of airways disease and emphysema. We observed that non-tumour lobe ventilation heterogeneity was related to pulmonary function test measurements. In addition, smoking history and airflow limitation independently provided a >93% classification rate for patients with ventilation abnormalities beyond the tumour suggesting that these measurements may be used to categorize NSCLC patients for functional lung avoidance radiation therapy schemes. Taken together these results suggest that COPD phenotypes provide a way to identify NSCLC patients for functional lung avoidance radiation therapy.

Conflict of interest

None.

References

[1] Kirby M, Mathew L, Wheatley A, Santyr GE, McCormack DG, Parraga G. Chronic obstructive pulmonary disease: longitudinal hyperpolarized (3)He MR imaging. Radiology 2010;256:280–9.

[2] Kirby M, Pike D, Coxson HO, McCormack DG, Parraga G. Hyperpolarized He ventilation defects used to predict pulmonary exacerbations in mild to moderate chronic obstructive pulmonary disease. Radiology 1401;2014:61.

[3] Kirby M, Mathew L, Heydarian M, Etemad-Rezai R, McCormack DG, Parraga G. Chronic obstructive pulmonary disease: quantification of bronchodilator effects by using hyperpolarized (3)He MR imaging. Radiology 2011;261:283–92.

[4] Coxson HO, Leipsic J, Parraga G, Sin DD. Using pulmonary imaging to move chronic obstructive pulmonary disease beyond FEV1. Am J Respir Crit Care Med 2014;190:135–44.

[5] Shioyama Y, Jang SY, Liu HH, Guerrero T, Wang X, Gayed IW, et al. Preserving functional lung using perfusion imaging and intensity-modulated radiation therapy for advanced-stage non-small cell lung cancer. Int J Radiat Oncol 2007;68:1349–58.

[6] Yaremko BP, Guerrero TM, Noyola-Martinez J, Guerra R, Lege DG, Nguyen LT, et al. Reduction of normal lung irradiation in locally advanced non-small-cell lung cancer patients, using ventilation images for functional avoidance. Int J Radiat Oncol 2007;68:562–71.

[7] Ding K, Bayouth JE, Buatti JM, Christensen GE, Reinhardt JM. 4DCT-based measurement of changes in pulmonary function following a course of radiation therapy. Med Phys 2010;37:1261–72.

[8] Vinogradskiy YY, Castillo R, Castillo E, Chandler A, Martel MK, Guerrero T. Use of weekly 4DCT-based ventilation maps to quantify changes in lung function for patients undergoing radiation therapy. Med Phys 2012;39:289–98.

[9] Hodge CW, Tome WA, Fain SB, Bentzen SM, Mehta MP. On the use of hyperpolarized helium MRI for conformal avoidance lung radiotherapy. Med Dosim 2010;35:297–303.

[10] Ireland RH, Bragg CM, McJury M, Woodhouse N, Fichele S, van Beek EJ, et al. Feasibility of image registration and intensity-modulated radiotherapy planning with hyperpolarized helium-3 magnetic resonance imaging for non-small-cell lung cancer. Int J Radiat Oncol Biol Phys 2007;68:273–81.

[11] Mathew L, Vandyk J, Etemad-Rezai R, Rodrigues G, Hyperpolarized Parraga G. (3)He pulmonary functional magnetic resonance imaging prior to radiation therapy. Med Phys 2012;39:4284–90.

[12] Christian JA, Partridge M, Nioutsikou E, Cook G, McNair HA, Cronin B, et al. The incorporation of SPECT functional lung imaging into inverse radiotherapy planning for non-small cell lung cancer. Radiother Oncol 2005;77:271–7.

[13] Marks LB, Spencer DP, Bentel GC, Ray SK, Sherouse GW, Sontag MR, et al. The utility of SPECT lung perfusion scans in minimizing and assessing the physiologic consequences of thoracic irradiation. Int J Radiat Oncol Biol Phys 1993;26:659–68.

[14] Jogi J, Jonson B, Ekberg M, Bajc M. Ventilation-perfusion SPECT with 99mTc-DTPA versus Technegas: a head-to-head study in obstructive and nonobstructive disease. J Nucl Med 2010;51:735–41.

[15] Mathew L, Wheatley A, Castillo R, Castillo E, Rodrigues G, Guerrero T, et al. Hyperpolarized (3)He magnetic resonance imaging: comparison with four-dimensional X-ray computed tomography imaging in lung cancer. Acad Radiol 2012;19:1546–53.

[16] Castillo R, Castillo E, Martinez J, Guerrero T. Ventilation from four-dimensional computed tomography: density versus Jacobian methods. Phys Med Biol 2010;55:4661.

[17] Guerrero T, Sanders K, Castillo E, Zhang Y, Bidaut L, Pan T, et al. Dynamic ventilation imaging from four-dimensional computed tomography. Phys Med Biol 2006;51:777.

[18] Bauman G, Puderbach M, Deimling M, Jellus V, Chefd'hotel C, Dinkel J, et al. Non-contrast-enhanced perfusion and ventilation assessment of the human lung by means of fourier decomposition in proton MRI. Magn Reson Med 2009;62:656–64.

[19] Fain S, Schiebler ML, McCormack DG, Parraga G. Imaging of lung function using hyperpolarized helium-3 magnetic resonance imaging: review of current and emerging translational methods and applications. J Magn Reson Imaging 2010;32:1398–408.

[20] Hoover DA, Capaldi DP, Sheikh K, Palma DA, Rodrigues GB, Dar AR, et al. Functional lung avoidance for individualized radiotherapy (FLAIR): study protocol for a randomized, double-blind clinical trial. BMC Cancer 2014;14:934.

[21] Miller MR, Hankinson J, Brusasco V, Burgos F, Casaburi R, Coates A, et al. Standardisation of spirometry. Eur Respir J 2005;26:319–38.

[22] Parraga G, Ouriadov A, Evans A, McKay S, Lam WW, Fenster A, et al. Hyperpolarized 3He ventilation defects and apparent diffusion coefficients in chronic obstructive pulmonary disease: preliminary results at 3.0 Tesla. Investig Radiol 2007;42:384–91.

[23] Kirby M, Owrangi A, Svenningsen S, Wheatley A, Coxson HO, Paterson NA, et al. On the role of abnormal DLCO in ex-smokers without airflow limitation: symptoms, exercise capacity and hyperpolarised helium-3 MRI. Thorax 2013;68:752–9.

[24] Kirby M, Heydarian M, Svenningsen S, Wheatley A, McCormack DG, Etemad-Rezai R, et al. Hyperpolarized 3He magnetic resonance functional imaging semiautomated segmentation. Acad Radiol 2012;19:141–52.

[25] Eisenhauer EA, Therasse P, Bogaerts J, Schwartz LH, Sargent D, Ford R, et al. New response evaluation criteria in solid tumours: revised RECIST guideline (version 1.1). Eur J Cancer 2009;45:228–47.

[26] Sheikh K, Paulin GA, Svenningsen S, Kirby M, Paterson NA, McCormack DG, et al. Pulmonary ventilation defects in older never-smokers. J Appl Physiol 2014;117:297–306.

[27] Schroeder JD, McKenzie AS, Zach JA, Wilson CG, Curran-Everett D, Stinson DS, et al. Relationships between airflow obstruction and quantitative CT measurements of emphysema, air trapping, and airways in subjects with and without chronic obstructive pulmonary disease. Am J Roentgenol 2013;201:W460–70.

[28] Hanley JA, McNeil BJ. The meaning and use of the area under a receiver operating characteristic (ROC) curve. Radiology 1982;143:29–36.

[29] Edge SB, Byrd DR, Compton CC, Fritz AG, Greene FL, Trotti A. AJCC Cancer Staging Manual. New York: Springer; 2010.

[30] Eidelman D, Saetta MP, Ghezzo H, Wang NS, Hoidal JR, King M, et al. Cellularity of the alveolar walls in smokers and its relation to alveolar destruction. Functional implications. Am Rev Respir Dis 1990;141:1547–52.

[31] Vestbo J, Hurd SS, Agusti AG, Jones PW, Vogelmeier C, Anzueto A, et al. Global strategy for the diagnosis, management, and prevention of chronic obstructive pulmonary disease: GOLD executive summary. Am J Respir Crit Care Med 2013;187:347–65.

[32] Galban CJ, Han MK, Boes JL, Chughtai KA, Meyer CR, Johnson TD, et al. Computed tomography-based biomarker provides unique signature for diagnosis of COPD phenotypes and disease progression. Nat Med 2012;18:1711–5.

[33] Kirby M, Owrangi A, Svenningsen S, Wheatley A, Coxson HO, Paterson NA, et al. On the role of abnormal DLCO in ex-smokers without airflow limitation: symptoms, exercise capacity and hyperpolarised helium-3 MRI. Thorax 2013.

[34] Mathew L, Kirby M, Etemad-Rezai R, Wheatley A, McCormack DG, Hyperpolarized Parraga G. (3)He magnetic resonance imaging: preliminary evaluation of phenotyping potential in chronic obstructive pulmonary disease. Eur J Radiol 2011;79:140–6.